FEEDBACK STABILIZATION OF THE AXISYMMETRIC INSTABILITY OF A DEFORMABLE TOKAMAK PLASMA

N. POMPHREY, S.C. JARDIN, D.J. WARD
Princeton Plasma Physics Laboratory,
Princeton University,
Princeton, New Jersey,
United States of America

ABSTRACT. The paper presents an analysis of the magnetohydrodynamic stability of the axisymmetric system consisting of a free boundary tokamak plasma with non-circular cross-section, finite resistivity passive conductors, and an active feedback system with magnetic flux pickup loops, a proportional amplifier with gain G and current carrying poloidal field coils. A numerical simulation of the system when G is set to zero identifies flux loop locations which correctly sense the plasma motion. However, when certain of these locations are incorporated into an active feedback scheme, the plasma fails to be stabilized, no matter what value of the gain is chosen. Analysis on the basis of an extended energy principle indicates that this failure is due to the deformability of the plasma cross-section.

1. INTRODUCTION

It is well known that tokamak plasmas with elongated cross-sections are subject to a pernicious axisymmetric magnetohydrodynamic (MHD) instability and must be stabilized by the placement of nearby passive conductors, and by an active feedback system which responds on the resistive time-scale of these conductors [1–8]. Most previous analyses of the stability of such a feedback system have considered the case of a deformable plasma stabilized by perfectly conducting passive conductors only [1, 3], or the case of a rigid filamentary plasma with resistive conductors and an active feedback system [2]. Here we discuss important new effects present in the more realistic configuration consisting of a finite-size deformable plasma, resistive conductors and an active feedback system. We also discuss the importance of the low frequency limit of this system in which the resistive conductors do not enter the analysis.

The components of an active feedback system include: (1) a means of observing the plasma motion, for example magnetic flux pickup loops, (2) a set of current carrying feedback coils positioned so that they produce a magnetic field which opposes the unstable plasma motion, and (3) an amplifier system which transforms the observed flux measurements into a voltage signal at the coils. It is clear that the placement of the feedback coils is important. However, we will show in this paper that the correct placement of the flux loops is also critical; despite a placement which correctly senses the vertical motion of the plasma, the instability may fail to be stabilized by any value of the gain. We demonstrate this effect by analysing the results of a numerical simulation relevant to the Princeton Beta Experiment (PBX) [9, 10]. We use Bode diagram and Nyquist techniques for the analysis. Similar results are found in an analytic calculation which applies the energy principle of ideal MHD to a straight plasma with rectangular cross-section and constant current density. The successful design of feedback systems for future experiments must consider the correct placement of flux pickup loops as a critical issue.

2. NUMERICAL SIMULATION RESULTS

Figure 1 shows a schematic of a shaped plasma for which position control is a necessary element of the design. The plasma carries 0.75 MA current and has a cross-section that is elongated and indented on the inboard side. Conducting plates surrounding the plasma lead to passive stabilization on the ideal MHD time-scale. The L/R time for the passive conductors is 100 ms. The poloidal field coil system used for equilibrium, shaping and feedback control is shown, as are two pairs of observation points. The flux difference between the top and bottom members of these pairs is a measure of the displacement of the

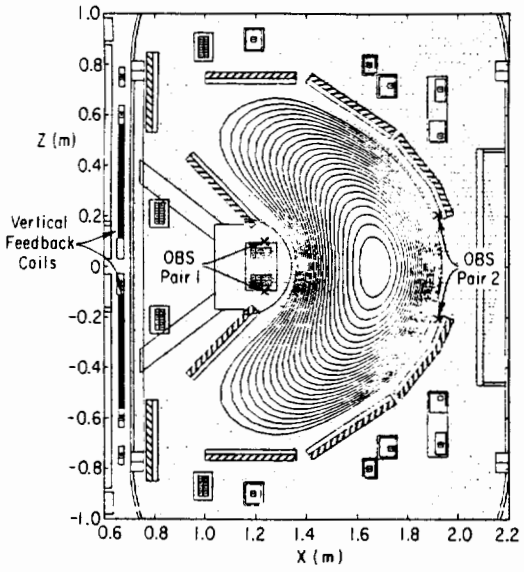

FIG. 1. Schematic of the Modified Princeton Beta Experiment (PBX-M). The inboard and outboard observation pairs used for feedback control in the numerical simulations are denoted by crosses.

plasma from its equilibrium position on a midplane. Apart from the location of these pickup loops, the system shown in Fig. 1 is an accurate representation of the modified Princeton Beta Experiment (PBX-M) [11].

We have used the Princeton Tokamak Simulation Code (TSC) [12] to analyse issues of vertical position control for the configuration described above. The TSC accurately models the transport time-scale evolution of axisymmetric plasmas, including the plasma interaction with passive and active feedback systems. For the simulations described below, we employ a simple feedback control law requesting an incremental current from the vertical feedback coils in proportion to the measured flux imbalance between one or other of the observation pairs, i.e.

$$I_W(t) = \beta \times [\psi_i^{top}(t) - \psi_i^{bottom}(t)] \qquad (1)$$

where i = 1 refers to the inboard observation pair and i = 2 refers to the outboard observation pair.

In the passive sense, the inboard observation pair and the outboard observation pair are equally good at detecting the vertical motion of the plasma. This is illustrated in Fig. 2, Case A, which shows the results of a simulation where the active feedback system is turned off by setting the gain β equal to zero. The flux differences $\Delta\psi_i(t) = \psi_i^{top}(t) - \psi_i^{bottom}(t)$ are plotted as a function of time for each observation pair. We see that the same growth rate for the instability is calculated by the TSC using either observation pair, and that the amplitude of the flux detected by each pair of loops is essentially the same, corresponding to a nearly rigid displacement. We now show that despite the fact that both observation pairs detect the unstabilized motion equally well, only the outboard pair can be successfully incorporated into the active feedback scheme defined by Eq. (1).

To investigate the stability of the feedback system, we adopt some techniques of control engineering [13]. Figure 3 is a block diagram for the system; it shows the relationship between components, and the flow of signals from input to output. A reference current signal is input in the vertical feedback coils, the plasma/conductor/vacuum MHD equations are advanced by the TSC, and the measured flux difference between a

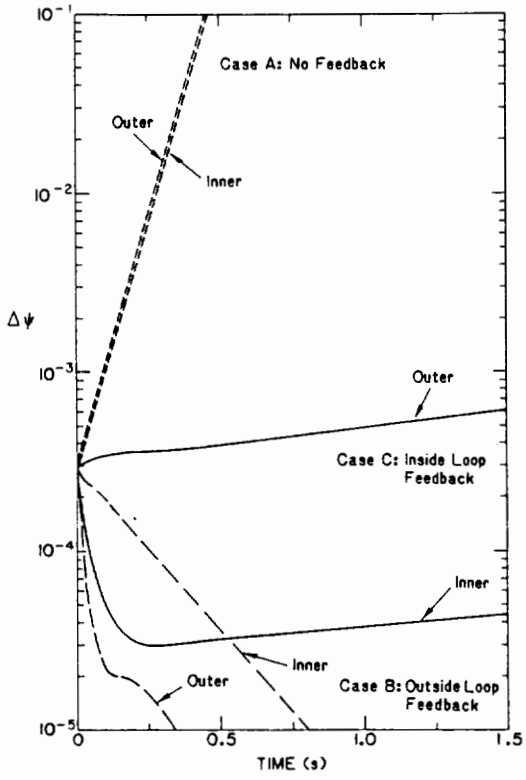

FIG. 2. Flux differences, $\Delta\psi_i(t) = \psi_i^{top}(t) - \psi_i^{bottom}(t)$, for the inner and outer observation pairs, plotted as a function of time.
Case A: Simulation results when the feedback gain β is zero. The same growth rate is obtained using either observation pair.
Case B: Active feedback with the feedback coils connected to the outside flux loops. The plasma is stable.
Case C: Active feedback with the feedback coils connected to the inside flux loops. The plasma is unstable.
The same feedback gain values were used in Cases B and C.

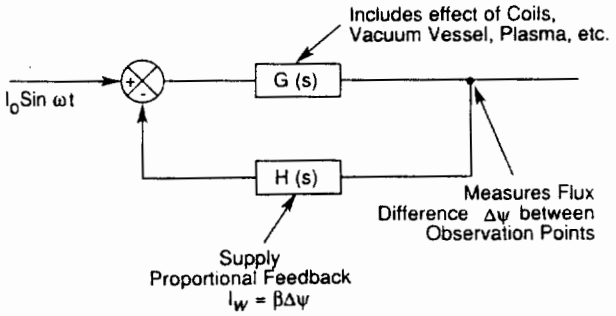

FIG. 3. Block diagram for the frequency response analysis of the control system.

pair of observation points is output. The feedback loop is closed by amplifying the output and returning it to the feedback coils as a current correction to the reference signal. For stability, all poles of the closed-loop transfer function, $T(s) = G(s)/[1 + \beta G(s)]$, must have negative real parts. The location of these poles is determined by the encirclement theorem, which leads to the Nyquist criterion for stability:

$$\frac{1}{2\pi}[\Delta \arg(1 + \beta G(s))]_{-i\infty}^{+i\infty} = N_p \qquad (2)$$

The phase change of the transfer function on the left-hand side can be interpreted as the number of counter-clockwise encirclements of the point (−1,0) by the $\beta G(s)$ locus as s is increased from $-i\infty$ to $+i\infty$, and N_p is the number of poles of $\beta G(s)$ having positive real parts. For a vertically unstable plasma partially stabilized by resistive walls, it is possible to show that $N_p = 1$.

The open-loop transfer function G(s) is not expressed in closed form for our problem and must be evaluated numerically. To do this, we input a test signal in the feedback coils in the form of a sinusoid with frequency ω. The steady state response characteristics of a stable system are such that $|\beta G(i\omega)|$ is equal to the amplitude ratio of the output and input sinusoids, and $\arg[\beta G(i\omega)]$ is the phase shift of the output sinusoid with respect to the input sinusoid. The data are collected on opposite sides of the summing point (see Fig. 3).

Figure 4 presents results obtained from running the TSC, using first the inboard observation pair and then the outboard observation pair for monitoring the flux. The sign and magnitude of the gain are the same for both cases. The results are shown as a Bode diagram, which consists of two graphs: one is a plot of $\log|\beta G(i\omega)|$ versus ω, the other is a plot of $\arg[\beta G(i\omega)]$ versus ω. Once the Bode diagram is constructed, the Nyquist plots follow readily. We see that use of the outboard observation pair gives rise to a closed curve which meets the conditions required by the Nyquist stability criterion. On the other hand, the Nyquist curve obtained using the inboard observation pair not only fails to enclose the point (−1,0) but is also described in the wrong sense. Since changing beta simply scales the distance of each point on a curve to the origin but leaves the sense of traversal unchanged, the feedback system which uses the outboard observation pair will be stable for a finite range of beta, corresponding to the enclosure of (−1,0), whereas the feedback system which uses the inboard observation pair will be unstable for all values of beta.

The essential difference in behaviour of the two feedback systems is the response to low frequencies. At very high frequency, the signal from the feedback coils is unable to affect the plasma motion because it cannot penetrate the intervening passive conductors. The feedback system is completely passive in this

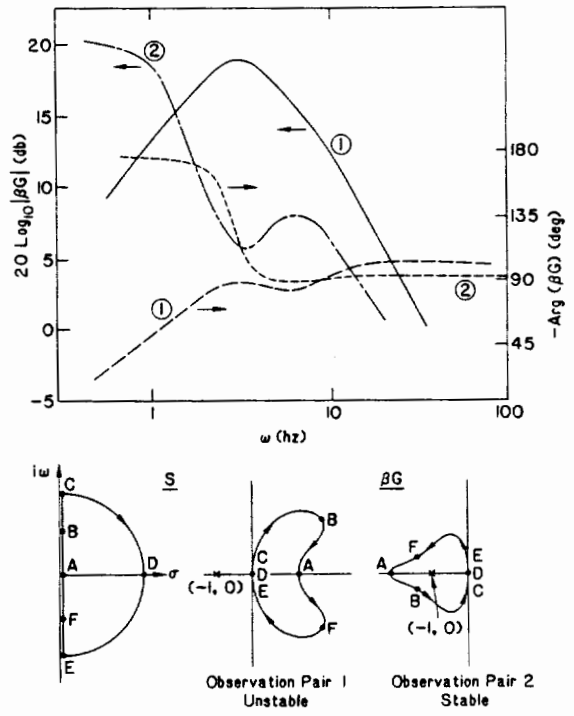

FIG. 4. Top: Frequency dependence of the amplitude and phase of the transfer function G when observation pairs 1 and 2 are used to monitor the flux.
Bottom: Nyquist curves resulting from the mapping to the complex G plane.

limit. If the frequency is lowered, to become comparable to the inverse L/R time of the conductors, the signal has time to influence the plasma motion. The influence is seen in the Bode plots as a dramatic change in slope in the curves of amplitude and phase. When the frequency is lowered towards the zero frequency limit, the contrast between the two observation points is most clear. In this limit, the passive stabilizers are completely transparent to the feedback signal and, therefore, cannot affect the feedback response of the plasma. It is in this low frequency limit that the placement of the flux detection loops can determine the overall stability of the system.

To further illustrate the effect seen in the Bode plots, we show two initial-value, time dependent simulations with the TSC using the same initial conditions for the plasma as in the passive calculation (Case A of Fig. 2), but with the feedback system activated and connected to the outside flux loops (Case B) or the inside flux loops (Case C). For each simulation the feedback gain had the same value as in the frequency domain analysis of Fig. 4. The results are shown in Fig. 2.

For Case B, where the feedback system is connected to the outer observation pair, the plasma motion is seen to be stabilized. The flux differences measured by the inner and the outer observation pairs both decrease with time, with the flux difference between the outer loops almost an order of magnitude less than the flux difference between the inner loops. This indicates some plasma distortion. For Case C, where the feedback system is connected to the inboard observation pair, the plasma remains unstable, albeit with a much reduced growth rate. The flux difference between the inner observation loops is now an order of magnitude less than the flux difference between the outer loops, also indicating a plasma distortion, but one whose detailed form is different compared with Case B.

In summary, the unstable eigenfunction depends on the position of the flux loops used to detect the motion, even though the feedback coils, in which the feedback currents appear, are exactly the same in the two cases. We now investigate stability in the low frequency limit with an analytic model.

3. ANALYTIC MODEL

A plasma column of a constant current density and square cross-section is unstable to a non-rigid axisymmetric (n = 0) instability [14]. Here we modify

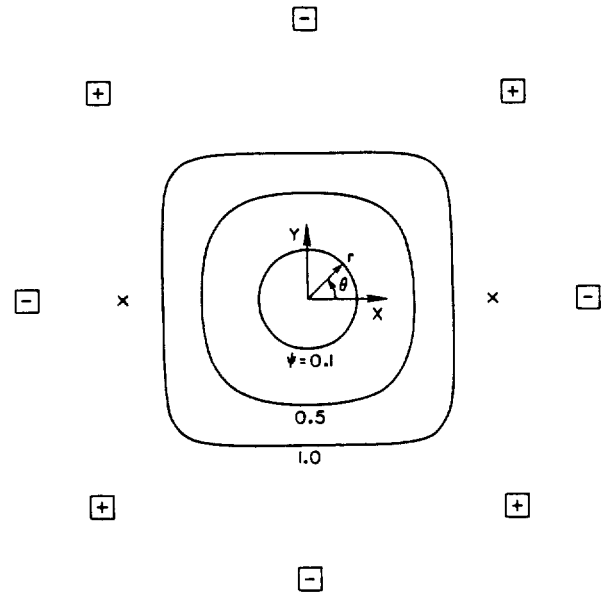

FIG. 5. Contours of constant flux for the analytic model. The equilibrium magnetic field is produced by coils which push on the sides and pull at the corners. A pair of crosses on the midplane denote a typical observation pair for monitoring the position instability.

the analysis of Ref. [14] to include an active feedback system and we show that there are forbidden regions for the placement of the pickup loops if stability is to be ensured. For the straight plasma, the equilibrium poloidal flux ψ satisfies $\nabla^2 \psi = j_z$. We choose j_z = constant, and

$$\psi = r^2 + \alpha r^4 \cos 4\theta \tag{3}$$

Here, α is a squareness parameter, which is assumed to be small. If $\alpha = 0$, then the plasma–vacuum interface ($\psi = 1$) is a circle. Even modest values of α, such as $\alpha = 0.2$, make the $\psi = 1$ surface nearly square. Figure 5 shows a schematic of the plasma, the poloidal field coils and typical pairs of observation coils.

The δW of the energy principle can be written as separate contributions from the plasma and from the vacuum:

$$2\delta W = \int_p [(\nabla \phi_p)^2 + j_z \xi \cdot \nabla \phi_p] dA$$

$$+ \int_v [(\nabla \phi_v)^2 + \phi_v \nabla^2 \phi_v] dA \tag{4}$$

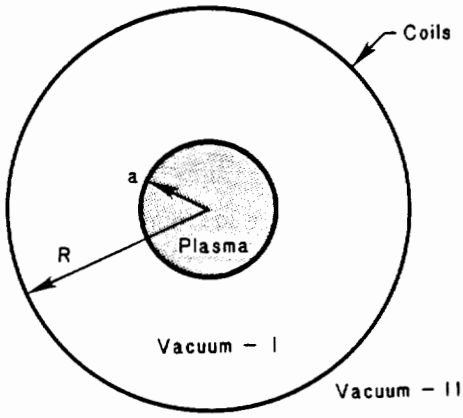

FIG. 6. Plasma and vacuum regions for the analytic calculation.

where ϕ is the perturbed flux function, ξ is the fluid displacement, and the subscripts p and v refer to plasma and vacuum, respectively. To evaluate this expression for the given model, it is convenient to express δW in terms of the flux co-ordinates (ψ,θ,z). Thus, we write

$$2\delta W = \int\int d\psi d\theta \mathcal{J}(\nabla\phi_p)^2 - j_z \oint d\theta \mathcal{J}\phi_p^2 - \oint d\theta \mathcal{J}\phi_v(\nabla\psi\cdot\nabla\phi_v) \tag{5}$$

where

$$(\nabla\phi_p)^2 = (\nabla\psi)^2\left(\frac{\partial\phi_p}{\partial\psi}\right)^2 + 2\nabla\psi\cdot\nabla\theta\left(\frac{\partial\phi_p}{\partial\psi}\right)\left(\frac{\partial\phi_p}{\partial\theta}\right) + (\nabla\theta)^2\left(\frac{\partial\phi_p}{\partial\theta}\right)^2 \tag{6}$$

and

$$\mathcal{J} = (\nabla\psi\cdot\nabla\theta\times\nabla z)^{-1} = \frac{1}{2}\frac{dr^2}{d\psi} \tag{7}$$

is the Jacobian. The integral denoted by $\oint$ is evaluated around the $\psi = 1$ contour, and $j_z = 4$ in the units of Eq. (3). Since α is small, Eq. (3) can be inverted to obtain $r(\psi,\theta)$, from which the metric elements and the Jacobian can be evaluated.

The procedure for evaluating δW follows the description given in Ref. [14], but with the perturbed vacuum flux modified by the presence of current carrying feedback coils. Figure 6 shows a schematic of the plasma and vacuum regions for the analytic calculation. The perturbed vacuum flux is given the following representation:

In region I,

$$\phi_v^I(r,\theta) = \sum_{m=1}^{\infty} B_m^I r^{-m}\cos m\theta + \sum_{m=1}^{\infty} L_m r^m \cos m\theta \tag{8}$$

In region II,

$$\phi_v^{II}(r,\theta) = \sum_{m=1}^{\infty} B_m^{II} r^{-m}\cos m\theta \tag{9}$$

The two vacuum regions are separated by a circular contour, of radius R, upon which the feedback coils lie. The second term in Eq. (8) is the multipolar decomposition of the flux from these coils. Each of the terms in the sum is interpreted as the flux from an 'equivalent feedback system' made up of m identical coils, equally spaced on the circular contour. The $m = 0$ terms in Eqs (8) and (9) are absent since they have zero gradient. In the plasma, the perturbed flux is given the form

$$\phi_p(\psi,\theta) = \sum_{m=0}^{\infty} D_m(\psi)\cos m\theta \tag{10}$$

Upon substituting Eqs (8)–(10) into Eq. (5) for δW, applying the appropriate matching conditions at the boundaries between regions I and II in the vacuum and at the plasma–vacuum interface (see Appendix), and repeated use of Euler's equation to minimize the plasma contributions to δW with respect to the Fourier coefficients, the following expressions for the energy and eigenfunction are obtained:

$$\frac{2\delta W}{\pi} = \alpha[-2D_1L_1^\alpha] + \alpha^2\left[-\frac{21}{4}D_1^2 + 4D_1D_3^\alpha + 4D_1D_5^\alpha + 2\sum_{m=1}^{\infty}(m-1)(D_m^\alpha)^2 - 2D_1L_1^{\alpha\alpha} + \frac{3}{2}D_1L_3^\alpha + \frac{5}{2}D_1L_5^\alpha - 2\sum_{m=1}^{\infty} mD_m^\alpha L_m^\alpha\right] \tag{11}$$

$$\xi_r^0 - 2\alpha r\xi_r^\alpha = -\frac{1}{2}D_1\cos\theta + \alpha\left[r\cos\theta D_1^\alpha + r^3\cos 3\theta\left(D_3^\alpha - \frac{7}{4}D_1\right) + r^5\cos 5\theta\left(D_5^\alpha + \frac{1}{4}D_1\right) + \sum_{m\neq 1,3,5}^{\infty} r^m\cos m\theta D_m^\alpha\right] \tag{12}$$

$$\xi_\theta^0 + 2\alpha r\xi_\theta^\alpha = +\frac{1}{2}D_1 \sin\theta$$

$$+ \alpha[r\sin\theta D_1^\alpha + r^3 \sin 3\theta(D_3^\alpha - \frac{7}{4}D_1)$$

$$+r^5 \sin 5\theta(D_5^\alpha + \frac{1}{4}D_1) + \sum_{m\neq 1,3,5}^{\infty} r^m \sin m\theta D_m^\alpha] \quad (13)$$

In these equations the Fourier coefficients D_m are evaluated at the plasma edge, $\psi = 1$. The alpha orderings are shown explicitly so that D_m^α represents the first-order piece of D_m, etc.

So far, we have not specified any details of the feedback system. By analogy with the numerical experiment reported in the previous section, we let each feedback system respond to the plasma motion by generating coil currents in proportion to some linear combination of perturbed flux. Schematically,

$$L_m = G_{mn}\Delta\phi_v(D_n) \quad (14)$$

If the gain matrix G has the correct symmetry properties (see Appendix), this form of feedback law can be shown to leave the stability operator self-adjoint, so that the energy principle will still apply. The gain elements G_{mn} should be at least of the order of α, so that the feedback system has no effect when α is zero. (A circular plasma is motionally stable.) Hence, $L_m^\alpha = G_{mn}^\alpha(\Delta\phi_v^0)$. Equation (8) for ϕ_v shows that $\Delta\phi_v^0$ is proportional to D_1, with a constant of proportionality that depends on the location of the observation points. If we absorb the constant of proportionality into the G-symbol for the gain, the first-order contribution to the energy becomes

$$\frac{2\delta W^\alpha}{\pi} = -2G_{11}^\alpha(D_1)^2 \quad (15)$$

Thus, to first order in α, the system stability depends only on the sign of G_{11}^α.

Suppose now that $L_1^\alpha = 0$. Then, δW^α vanishes, and stability is determined by the second-order terms in δW. To simplify the analysis of $\delta W^{\alpha\alpha}$, we choose a simplified feedback model motivated by the form of the eigenfunction without feedback: Since the zeroth-order displacement eigenfunction is a rigid shift, it is appropriate to set the rigid shift component of the first-order displacement equal to zero, i.e. $D_1^\alpha = 0$. When δW is minimized with respect to the D_m's, we obtain $D_3^\alpha = -\frac{1}{2}D_1$, $D_5^\alpha = -\frac{1}{4}D_1$ and $D_m^\alpha = 0$ for $m \neq 3, 5$. The minimizing eigenfunction (first order) is, therefore,

$$\xi_r^\alpha = \frac{9}{8}r^2 D_1 \cos 3\theta \ , \ \xi_\theta^\alpha = -\frac{9}{8}r^2 D_1 \sin 3\theta \quad (16)$$

which is an m = 3 wrinkle superimposed on the rigid shift [14]. The simplest non-trivial feedback model we can choose to make δW self-adjoint (see Appendix) is, therefore,

$$L_1^{\alpha\alpha} = G_{11}^{\alpha\alpha}D_1 + G_{13}^\alpha D_3^\alpha$$

$$L_3^\alpha = \frac{1}{3}G_{13}^\alpha D_1 \quad (17)$$

$$L_m^\alpha = 0 \qquad m > 3$$

This corresponds to coils with an ability to respond (on account of the flux measurements) to both the rigid shift and the m = 3 perturbations.

We substitute these feedback terms into the expression for δW, Eq. (11). For a trial displacement, we use the eigenfunction found for the system without feedback, given in Eq. (16). The calculated δW with the feedback terms included is

$$\frac{2\delta W}{\pi} = \alpha^2 D_1^2[-\frac{27}{4} - 2G_{11}^{\alpha\alpha} + \frac{5}{2}G_{13}^\alpha] \quad (18)$$

Without feedback ($G_{11}^{\alpha\alpha} = G_{13}^\alpha = 0$), the plasma is seen to be unstable. With feedback, δW can be made positive for a range of values of the gain coefficients. Specifically, for any choice of G_{13}^α, a $G_{11}^{\alpha\alpha}$ can be found which is stabilizing. The converse is also true. This can be seen in Fig. 7, which gives the stability boundary for this trial displacement in $(G_{11}^{\alpha\alpha}, G_{13}^\alpha)$ parameter space.

Now let us consider the effect of the feedback system on the eigenfunction. We take our expression for δW, Eq. (11), with the feedback terms included and minimize with respect to the D_m^α. This yields $D_3^\alpha = [-\frac{1}{2} + \frac{1}{2}G_{13}^\alpha]D_1$, $D_5^\alpha = -\frac{1}{4}D_1$ and $D_m^\alpha = 0$ for $m \neq 3, 5$.

The minimized δW is

$$\frac{2\delta W}{\pi} = \alpha^2 D_1^2[-\frac{27}{4} - 2G_{11}^{\alpha\alpha} + \frac{5}{2}G_{13}^\alpha - (G_{13}^\alpha)^2] \quad (19)$$

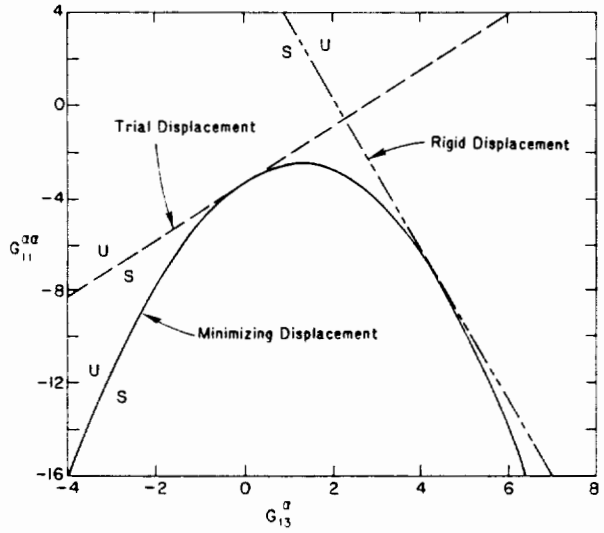

FIG. 7. Stable and unstable regions for a range of values of the gains $G_{11}^{\alpha\alpha}$ and G_{13}^{α}. The long-dashed line represents the stability boundary for the trial displacement given in Eq. (16). The short-dashed line represents the stability boundary for the rigid displacement. The solid curve denotes the stability boundary for the minimized eigenfunction that is deformed by the feedback system. The regions in the $(G_{11}^{\alpha\alpha}, G_{13}^{\alpha})$ parameter space where the plasma is stable or unstable are marked on either side of the stability boundary by S and U, respectively.

with the corresponding (first-order) eigenfunction

$$\xi_r^{\alpha} = D_1 r^2 \left(\frac{9}{8} - \frac{G_{13}^{\alpha}}{4}\right) \cos 3\theta$$
$$\xi_\theta^{\alpha} = -D_1 r^2 \left(\frac{9}{8} - \frac{G_{13}^{\alpha}}{4}\right) \sin 3\theta \qquad (20)$$

The last two terms in δW are seen to be stabilizing for $0 < G_{13}^{\alpha} < 5/2$, and optimally stabilizing for $G_{13}^{\alpha} = 5/4$. For this optimal value, the mode is stabilized if $G_{11}^{\alpha\alpha} < 83/32$. This is summarized in Fig. 7, which shows the stable and unstable boundaries for this minimized δW in the $(G_{11}^{\alpha\alpha}, G_{13}^{\alpha})$ parameter space. It is seen that for any choice of G_{13}^{α}, a $G_{11}^{\alpha\alpha}$ can be found which stabilizes the mode. However, the converse is not true, and the choice of $G_{11}^{\alpha\alpha}$ is critical. Since the actual values of the G-gains depend on the location of the observation points, we see that this result translates into a criticality for the placement of the flux pickup loops.

It is also interesting to consider the conclusions that result from restricting the instability to take the form of a rigid displacement. These indicate that the above behaviour is due to the ability of the feedback systems to distort the eigenfunction. For a rigid displacement, we must choose (see Eq. (12)) $D_3^{\alpha} = \frac{7}{4} D_1$, $D_5^{\alpha} = -\frac{1}{4} D_1$ and $D_m^{\alpha} = 0$ for $m \neq 3, 5$. Then the expression for δW becomes

$$\frac{2\delta W}{\pi} = \alpha^2 D_1^2 \left[\frac{27}{2} - 2G_{11}^{\alpha\alpha} - \frac{13}{2} G_{13}^{\alpha}\right] \qquad (21)$$

The stable and unstable regions for this rigid instability are also shown in Fig. 7. Because of the linearity of δW on the G's, it follows that a $G_{11}^{\alpha\alpha}$ can be found to stabilize the mode for any value of G_{13}^{α}. The converse is also true. Therefore, for a rigid instability, the detailed placement of flux pickup loops for monitoring the motion is not critical. Note that the stable/unstable boundary for the rigid instability encloses the stable region for the deformable instability, except for a common point at $G_{13}^{\alpha} = 9/2$. Equation (20) shows that for this value of the gain, G_{13}^{α}, the eigenfunction no longer supports an $m = 3$ deformation, so that the eigenfunctions for the rigid and deformable instability coincide.

The stable/unstable boundary for the trial displacement, given by Eq. (16), also encloses the stable region for the deformable instability. It is clear that the minimizing eigenfunction, Eq. (20), is affected by the feedback and this results in a plasma that can only be stabilized by feedback where the gain $G_{11}^{\alpha\alpha}$ lies within a restricted region. Thus we see that the feedback system with certain placements of the observation points can allow the unstable eigenfunction to deform so that the plasma will remain unstable.

4. CONCLUSIONS

We have demonstrated the usefulness of a new technique for analysing the stability and control properties of an axisymmetric tokamak using the time dependent simulation code TSC to perform frequency domain analysis. Using this technique, we find that in the PBX-M tokamak, certain placements of the magnetic pickup coils, on the inboard side, lead to an unstable system, regardless of the gain, whereas other placements, on the outboard side, will give a stable system for sufficiently large values of the gain. A simplified analytic model suggests that this behaviour results from the non-rigid deformable nature of the plasma cross-section and from the plasma's ability to modify its unstable eigenfunction

according to the particular feedback system. No such effect is present when the plasma is modelled as a current filament, a finite size rigid conductor or a 'trial function' displacement determined in the absence of feedback.

We can interpret this phenomenon qualitatively in terms of a simple physical picture. As part of the plasma instability, a perturbed magnetic field is produced in the vacuum region and this is sensed by the magnetic pickup coils. If the plasma is unstable enough, it can modify its eigenfunction to deform its cross-section so that a null in the perturbed vacuum magnetic field will appear at the position of the observation loops. Since these loops will then be unable to detect the plasma instability, the feedback system will be rendered inoperative.

We also emphasize the importance of the two limiting cases for stability analysis of this system. For frequencies that are large compared to the plate resistive times, we can treat the plates as perfect conductors, neglect the active feedback system and perform standard ideal MHD analysis of the system. In the opposite limit – that of very low frequencies – the conducting plates are transparent and do not enter the analysis. In this limit, the system must be considered as consisting only of a deformable plasma and active feedback.

Appendix

SELF-ADJOINTNESS OF δW IN THE PRESENCE OF A FEEDBACK SYSTEM

Since the first two terms in the expression for δW, Eq. (5), are manifestly self-adjoint, our discussion can be limited to the vacuum contribution

$$\delta W_v = -\oint d\theta \mathcal{J} \phi_v (\nabla\psi \cdot \nabla\phi_v)$$

$$= \int_v [(\nabla\phi_v)^2 + \phi_v \nabla^2 \phi_v] dA \qquad (A.1)$$

The first term on the right-hand side of Eq. (A.1) is again clearly self-adjoint. In the second term, let

$$\phi_v = \sum_{m=0}^{\infty} \phi_v^m(r) \cos m\theta \qquad (A.2)$$

Also, let the feedback coils be located in the vacuum at a radius r = R. Then

$$\nabla^2 \phi_v = \sum_{m=0}^{\infty} \frac{1}{\pi R} \delta(r - R) J_0^m \cos m\theta \qquad (A.3)$$

Using Eqs (A.3) and (A.2), the second term of Eq. (A.1) becomes

$$\delta W_v^{(2)} = \sum_{m=1}^{\infty} \phi_v^m(R) J_0^m \qquad (A.4)$$

Consider now a feedback law which relates the coil currents to the perturbed flux at the coils according to

$$J_0^m = \sum_{n=1}^{\infty} g_{mn} \phi_v^n(R) \qquad (A.5)$$

We see that if the gain matrix g_{mn} is symmetric, i.e.

$$g_{mn} = g_{nm} \qquad (A.6)$$

then $\delta W_v^{(2)}$, and hence δW_v, is self-adjoint.

The symmetry restriction on g_{mn} constrains the relationship between the feedback currents L_m and the Fourier coefficients D_m of the perturbed flux on the plasma–vacuum boundary. This relationship is obtained in two stages. In the first stage, the matching conditions for the vacuum flux are applied at the boundary between regions I and II in the vacuum (see Fig. 6). In the second stage, the matching conditions are applied at the plasma–vacuum interface.

Stage 1

Continuity of ϕ_v at r = R gives

$$B_m^I + L_m R^{2m} = B_m^{II} \qquad (A.7)$$

while the jump condition for $\partial\phi_v/\partial r$ at r = R (see Eq. (A.3)) is

$$B_m^I - L_m R^{2m} = B_m^{II} + \frac{J_0^m R^m}{m\pi} \qquad (A.8)$$

Thus,

$$L_m = -\frac{R^{-m}}{2\pi m} J_0^m \qquad (A.9)$$

Inserting Eq. (A.9) into Eq. (8) of Section 3, using definition (A.5), and then solving for $\phi_v^m(r)$ at r = R gives

$$\phi_v^m(R) = [\delta_{mn} + \frac{1}{2\pi m} g_{mn}]^{-1} B_n^I R^{-n} \qquad (A.10)$$

If, now, we define the matrix

$$C_{mn} = -\frac{R^{-m}}{2\pi m} g_{mn} R^{-n} [\delta_{mn} + \frac{1}{2\pi m} g_{mn}]^{-1} \qquad (A.11)$$

then Eq. (A.9) relates the region I vacuum coefficients B_m^I to the feedback currents L_m, according to

$$L_m = C_{mn} B_n^I \qquad (A.12)$$

Stage 2

Continuity of flux across the plasma-vacuum interface implies that

$$\sum_{m=0}^{\infty} D_m \cos m\theta = \sum_{m=1}^{\infty} B_m^I r^{-m} \cos m\theta + \sum_{m=1}^{\infty} L_m r^m \cos m\theta \qquad (A.13)$$

where

$$r^m = 1 - \frac{m}{2} \alpha \cos 4\theta \qquad at \ \psi = 1 \qquad (A.14)$$

Equating Fourier coefficients on each side of Eq. (A.13), solving for B_m^I in terms of D_m and L_m, and substituting into Eq. (A.12) gives the matrix equation

$$L_m = G_{mn} D_m \qquad (A.15)$$

For the simplified 2 X 2 feedback system discussed in Section 3, the restriction that g_{mn} is symmetric to make δW self-adjoint, leads to Eq. (17).

ACKNOWLEDGEMENTS

It is a pleasure to acknowledge stimulating conversations and continuing encouragement from Drs K. Bol, M. Okabayashi, M. Reusch, and others in the PBX group.

This work was supported by the United States Department of Energy, under Contract No. DE-AC02-76-CHO-3073. One of the authors (DJW) was supported by the United States Air Force under its Laboratory Graduate Fellowship Program.

REFERENCES

[1] LAVAL, G., PELLAT, R., SOULE, J.S., Phys. Fluids **17** (1974) 835.
[2] JARDIN, S.C., LARRABEE, D.A., Nucl. Fusion **22** (1982) 1095.
[3] JARDIN, S.C., Phys. Fluids **21** (1978) 1851.
[4] LIPSCHULTZ, B., PRAGER, S.C., TODD, A., DeLUCIA, J., Nucl. Fusion **20** (1980) 683.
[5] TAKAHASHI, H., BOL, K., MAEDA, H., et al., Nucl. Fusion **22** (1982) 1597.
[6] YOKOMIZO, H., McCLAIN, F.W., JENSEN, T.H., Nucl. Fusion **23** (1983) 1593.
[7] WESSON, J.A., Nucl. Fusion **18** (1978) 87.
[8] REBHAN, E., SALAT, A., Nucl. Fusion **18** (1978) 1431.
[9] BOL, K., CHANCE, M., DEWAR, R., et al., PBX: the Princeton Beta Experiment, Rep. PPPL-2032, Princeton Plasma Physics Laboratory, Princeton, NJ (Sep. 1983).
[10] JARDIN, S.C., DeLUCIA, J., OKABAYASHI, M., et al., Nucl. Fusion **27** (1987) 569.
[11] MATERNA, P., CHRZANOWSKI, J., HOMAN, F., in Fusion Engineering (Proc. 12th Symp. Monterey, CA, 1987), IEEE, New York (1987) 346.
[12] JARDIN, S.C., POMPHREY, N., DeLUCIA, J., J. Comput. Phys. **66** (1986) 481.
[13] OGATA, K., Modern Control Engineering, Prentice-Hall, Inc., Englewood Cliffs, NJ (1970).
[14] ROSEN, M.D., Phys. Fluids **18** (1975) 482.

(Manuscript received 10 August 1988
Final manuscript received 16 December 1988)